

Vibronic coupling in asymmetric bichromophores: Theory and application to diphenylmethane

Ben Nebgen, Frank Lee Emmert, and Lyudmila V. Slipchenko

Citation: *J. Chem. Phys.* **137**, 084112 (2012); doi: 10.1063/1.4747336

View online: <http://dx.doi.org/10.1063/1.4747336>

View Table of Contents: <http://jcp.aip.org/resource/1/JCPSA6/v137/i8>

Published by the [American Institute of Physics](#).

Additional information on *J. Chem. Phys.*

Journal Homepage: <http://jcp.aip.org/>

Journal Information: http://jcp.aip.org/about/about_the_journal

Top downloads: http://jcp.aip.org/features/most_downloaded

Information for Authors: <http://jcp.aip.org/authors>

ADVERTISEMENT



AIP Advances

Special Topic Section:
PHYSICS OF CANCER

Why cancer? Why physics? [View Articles Now](#)

Vibronic coupling in asymmetric bichromophores: Theory and application to diphenylmethane

Ben Nebgen, Frank Lee Emmert III, and Lyudmila V. Slipchenko

Department of Chemistry, Purdue University, West Lafayette, Indiana 47907, USA

(Received 15 May 2012; accepted 7 August 2012; published online 30 August 2012)

The theory for modeling vibronic interactions in bichromophores was introduced in sixties by Witkowski and Moffitt [J. Chem. Phys. **33**, 872 (1960)] and extended by Fulton and Gouterman [J. Chem. Phys. **35**, 1059 (1961)]. The present work describes extension of this vibronic model to describe bichromophores with broken vibrational symmetry such as partly deuterated molecules. Additionally, the model is extended to include inter-chromophore vibrational modes. The model can treat multiple vibrational modes by employing Lanczos diagonalization procedure of sparse matrices. The developed vibronic model is applied to simulation of vibronic spectra of flexible bichromophore diphenylmethane and compared to high-resolution experimental spectra [J. A. Stearns, N. R. Pillsbury, K. O. Douglass, C. W. Müller, T. S. Zwier, and D. F. Plusquellic, J. Chem. Phys. **129**, 224305 (2008)]. © 2012 American Institute of Physics. [<http://dx.doi.org/10.1063/1.4747336>]

I. INTRODUCTION

The interaction of light and matter is a fundamental phenomenon whose understanding and control are quintessential for advances in science and technology. Often, quantum-mechanical treatment of the light-induced processes can be simplified by separating electronic and nuclear degrees of freedom by introducing the conventional Born-Oppenheimer (BO) approximation.¹ Yet, to explain processes such as conversion of solar to electrical energy as occurs in photosynthetic centers of plants and bacteria and is mimicked in photovoltaic devices, the electronic and nuclear motions cannot be uncoupled such that the BO approximation should be abandoned. A wide variety of classical, semi-classical, and quantum techniques have been suggested to simulate dynamics in such systems.² In classical approaches the nuclear wavepacket is approximated by an ensemble of particles that follow classical trajectories. Semi-classical methods add some missing quantum effects to this picture by allowing transitions between the electronic states, for example, through surface hopping³ or using the mean-field approximation.^{4,5} In quantum-dynamics methods the nuclear wavepacket is described by including quantum effects, such as interference between different parts of the packet.^{6,7}

Alternatively, one can circumvent complexities associated with modeling dynamics of vibronic systems and describe their vibronic spectra statically. This can be accomplished by solving the time-independent Schrodinger equation with an electronic-nuclear Hamiltonian. The present work applies the latter (static) approach to a molecular system composed of two (nearly) identical chromophores. Such bichromophores or molecular dimers have nearly degenerate electronic energy levels with an energy splitting close to the separation in vibrational energy levels, resulting in coupling of the electronic and nuclear degrees of freedom. Pioneering work in this direction was done by Witkowski and Moffitt,⁸ who derived the Hamiltonian for a dimer with a

specific symmetry element exchanging the monomers. This vibronic model was expanded on by Fulton and Gouterman (FG)^{9,10} by describing excited state vibrations through a series of displaced harmonic oscillators.^{10,11} Following this initial work, Siebrand and co-workers extended the theory to Raman scattering¹² and made connections to molecular aggregates.¹³ Since then, this model has been applied to a number of molecular dimers,¹⁴⁻¹⁹ extended to include multiple vibrational modes,²⁰⁻²² and used to describe vibronic states in more complex molecular aggregates.^{23,24}

The original FG vibronic coupling model is limited to cases where the dimer has a symmetry element interchanging the Hamiltonians of monomers. The symmetry element simplifies the dimer Hamiltonian and its numerical solution. However, at the expense of increased computational complexity, the Hamiltonian can be left in the asymmetric form and, after expanding the vibrational wavefunction in a basis, diagonalized numerically using the iterative Lanczos diagonalization routine, as previously suggested by Domcke and co-workers.²⁵ This approach can handle asymmetries in the vibrational wavefunction arising from partial deuteration. The present work describes an extension of the vibronic model to the asymmetric bichromophores of this type. The present work assumes that the bichromophore retains symmetry of the electronic wavefunction. However, with evaluation of an additional electronic integral this model can be generalized to molecules with asymmetries in electronic wavefunction arising, for example, from asymmetric molecular orientations, substituent groups on monomers, or from different interaction of monomers with environment, as would occur in realistic biological or materials systems. The present work also introduces the Hamiltonian for the inter-chromophore vibrational modes, i.e., vibrations that occur between the chromophores themselves. The inter-monomer Hamiltonian is fundamentally different from the intra-monomer one because the electronic coupling depends on the distance and orientation

between the two monomers and thus upon the inter-monomer vibrations.

Developments described in the present study differentiate from the previously reported extensions of the original FG vibronic model in several important aspects. For example, while the FG model was previously extended to simulate several vibrational modes,²⁰⁻²² our implementation utilizes the iterative Lanczos diagonalization routine that allows simultaneous modeling of a larger number of vibrations. The previous work on asymmetric dimers¹⁸ was focused on electronic asymmetries while maintaining the assumption of vibrational symmetry. This is in contrast to our model that targets vibrational rather than electronic asymmetry. There are also reports on modeling inter-monomer vibrations,^{17,18} which, however, do not include the explicit modulation of the exciton coupling matrix element along an inter-monomer mode. Our work presents a general approach for modeling the inter-monomer vibrations and explicitly includes a change of the electronic coupling along these modes.

To characterize the developed model, a series of model spectra are produced and analyzed. As an initial test, the extended vibronic coupling model is applied to vibronic spectra of flexible bichromophore diphenylmethane (DPM), which has been the subject of several spectroscopic studies over the last half century.²⁶⁻³⁰ Application to this symmetric molecule demonstrates the validity of the inter-monomer mode Hamiltonian and tests the asymmetric model in the symmetric limit. Our future work will focus on modeling vibronic spectrum of partially deuterated DPM (d5-DPM) that will fully utilize asymmetric aspects of the developed model.

II. THEORY

For a bichromophore (also called dimer) composed of two (nearly) identical monomers, the Hamiltonian can be written as a sum of the monomer Hamiltonians and electronic coupling $V_{AB}(L)$ and kinetic energy T_L terms

$$H = H_A + H_B + V_{AB}(L) + T_L. \quad (1)$$

The electronic coupling and the kinetic energy terms depend on the vector of six inter-monomer vibrational modes L . In this treatment, the electronic wavefunction of the dimer is not antisymmetrized, i.e., the electron exchange between the two monomers is neglected. This is a reasonable assumption for a large class of molecules, especially when monomers are spatially separated. However, the following derivations remain true even if the electronic wavefunction of the dimer is antisymmetrized, as is the case for bichromophores. Antisymmetrization of the electronic wavefunction affects the electronic coupling V_{AB} term that will include not only Coulomb but also exchange component.

Vibrations considered in this model are divided into intra-monomer and inter-monomer vibrations. Intra-monomer modes have kinetic and potential energy terms located within H_A and H_B and thus can be computed by calculations on either monomer. The inter-monomer modes are vibrations along the L vector introduced above. Typically, the inter-monomer modes have much lower frequencies than the intra-monomer modes. They cannot be obtained from monomer properties

but require (partial) knowledge of the dimer Hessian. Because of these principal differences, the treatment of the intra- and inter-monomer modes in the model should be different. Note that only the intra-monomer modes were considered in the original model and most extensions. The current paper provides the first systematic extension of the dimer vibronic coupling model to the inter-monomer vibrations.

A. Intra-monomer modes

Main steps of the symmetric dimer vibronic coupling model are repeated here in order to introduce notations and bring into context our developments. For the intra-monomer modes, the Hamiltonian of monomer A (and analogously for monomer B) is written as a sum of the vibrational kinetic energy term $T_A(Q_A)$ and the electronic Hamiltonian $h_A(q_A; Q_A)$,

$$H_A = h_A(q_A; Q_A) + T_A(Q_A). \quad (2)$$

The electronic Hamiltonian depends explicitly on the electron coordinate (q_A) and parametrically on the nuclear coordinate (Q_A) of monomer A. Let $\{\psi_i^{\text{el}}(q_A; Q_A)\}_{i \geq 0}$ be the eigenvectors of the electronic Hamiltonian h_A with energies $E_i(Q_A)$; $\{\phi_j(Q_A)\}_{j \geq 0}$ be the eigenvectors of the vibrational Hamiltonian $E_i(Q_A) + T_A(Q_A)$. Since similar relationships hold for monomer B, $H_A + H_B$ will satisfy the eigenvalue problem

$$\begin{aligned} (H_A + H_B)\psi_i^{\text{el}}(q_A; Q_A)\phi_n(Q_A)\psi_j^{\text{el}}(q_B; Q_B)\phi_m(Q_B) \\ = E_{i,j,n,m}(Q_A, Q_B)\psi_i^{\text{el}}(q_A; Q_A)\phi_n(Q_A) \\ \times \psi_j^{\text{el}}(q_B; Q_B)\phi_m(Q_B), \end{aligned} \quad (3)$$

where

$$E_{i,j,n,m}(Q_A, Q_B) = E_{i,n}(Q_A) + E_{j,m}(Q_B), \quad (4)$$

i and j represent the level of electronic excitation on monomers A and B, respectively. Similarly, n and m represent the vibrational excitation on either monomer.

Before introducing the electronic coupling, the energies obey the following relation:

$$E_{i,j,n,m} = E_{j,i,m,n}. \quad (5)$$

The degeneracy in the electronic states is split by the electronic coupling term $V_{AB}(L)$ in the electronic Hamiltonian Eq. (1).

Consider now a pair of exciton states. The excitation may occur either on monomer A or monomer B; neither double excitations (both on A and B) nor charge-transfer excitations (electron moves from A to B or vice versa) are considered in this model. Thus, a two element basis is sufficient for the electronic wavefunction

$$\begin{aligned} \{\pi_A^{(1)} = \psi_1^{\text{el}}(q_A; Q_A)\psi_0^{\text{el}}(q_B; Q_B), \\ \pi_B^{(1)} = \psi_0^{\text{el}}(q_A; Q_A)\psi_1^{\text{el}}(q_B; Q_B)\}. \end{aligned} \quad (6)$$

Though the following derivations are valid for any electronic states in the monomer, for the sake of simplicity, we use the notations corresponding to the electronic transition from the ground state ψ_0 to the first electronic excited state ψ_1 .

To find algebraic expressions for the vibrational energies, the Hamiltonian has to be expanded in the electronic basis, resulting in the following matrix elements:

$$\begin{aligned} \langle \pi_A^{(1)} | H | \pi_A^{(1)} \rangle &= T_A + E^{(1)}(Q_A) + T_B \\ &+ E^{(0)}(Q_B) + \langle \pi_A^{(1)} | V_{AB} | \pi_A^{(1)} \rangle, \end{aligned} \quad (7)$$

$$\begin{aligned} \langle \pi_B^{(1)} | H | \pi_B^{(1)} \rangle &= T_A + E^{(0)}(Q_A) + T_B \\ &+ E^1(Q_B) + \langle \pi_B^{(1)} | V_{AB} | \pi_B^{(1)} \rangle, \\ \langle \pi_A^{(1)} | H | \pi_B^{(1)} \rangle &= \langle \pi_B^{(1)} | H | \pi_A^{(1)} \rangle = \langle \pi_A^{(1)} | V_{AB} | \pi_B^{(1)} \rangle. \end{aligned} \quad (8)$$

In case of the intra-monomer modes, $V_{AB}(L)$ is expanded in Taylor series about the equilibrium position of $L = 0$ and only the zero-order term is kept:

$$\begin{aligned} \langle \pi_A^{(1)} | V_{AB}(L) | \pi_B^{(1)} \rangle &\simeq \langle \pi_A^{(1)} | V_{AB}(0) | \pi_B^{(1)} \rangle \\ &+ \frac{\partial}{\partial L} \langle \pi_A^{(1)} | V_{AB}(L) | \pi_B^{(1)} \rangle \Big|_{L=0} L \\ &+ \frac{\partial^2}{\partial^2 L} \langle \pi_A^{(1)} | V_{AB}(L) | \pi_B^{(1)} \rangle \Big|_{L=0} \frac{L^2}{2}. \end{aligned} \quad (9)$$

The remaining terms in the Taylor expansion along with the T_L term will be considered in Sec. II B regarding inter-monomer modes, since such vibrations affecting the relative positioning of the monomers are anticipated to have a large effect on coupling constant. Assuming the harmonic approximation for the potential energy surface (PES) in the vicinity of the minimum provides a functional form for $E^{(0)}(Q_A)$,

$E^{(1)}(Q_A)$, $E^{(0)}(Q_B)$, and $E^{(1)}(Q_B)$. For example, for monomer A,

$$E^{(0)}(Q_A) = \frac{1}{2} M \omega_A^2 Q_A^2, \quad (10)$$

$$E^{(1)}(Q_A) = E_e + l_A Q_A + \frac{1}{2} M \omega_A^2 Q_A^2, \quad (11)$$

where M is the reduced mass and ω is the characteristic frequency of the normal mode. The displacement l_A is defined as

$$l_A = dQ M \omega_A^2, \quad (12)$$

dQ is the displacement along the normal mode between geometries of the ground and excited states (see Fig. 1). For simplicity $Q_A = 0$ is defined as the equilibrium position for the normal mode in the ground electronic state, such that a linear term is only present in the expression for the excited state potential energy surface.

The integral $\langle \pi_A^{(1)} | V_{AB} | \pi_A^{(1)} \rangle$ in Eq. (7) can be evaluated from standard electronic structure packages by modifications of the electronic structure integral codes. Input of this integral is one of the requirements to handling electronic wavefunction asymmetry. However, this term is not necessary for bichromophores with symmetric electronic wavefunction since, by symmetry,

$$\langle \pi_A^{(1)} | V_{AB} | \pi_A^{(1)} \rangle = \langle \pi_B^{(1)} | V_{AB} | \pi_B^{(1)} \rangle. \quad (13)$$

Thus, these terms shift all energy levels by the same quantity and do not affect energy spacings. Leutwyler and co-workers studied electronic wavefunction asymmetry in the 2-pyridone · 6-methyl-2-pyridone dimer by adding these terms to the Hamiltonian matrix.¹⁸

To summarize, the Hamiltonian in the electronic basis can be written as

$$H = \begin{pmatrix} \frac{P_A^2}{2M} + E_A + l_A Q_A + \frac{1}{2} M \omega_A^2 Q_A^2 + \frac{P_B^2}{2M} + \frac{1}{2} M \omega_B^2 Q_B^2 & V_{AB} \\ V_{AB} & \frac{P_B^2}{2M} + \frac{1}{2} M \omega_B^2 Q_B^2 + \frac{P_A^2}{2M} + E_B + l_B Q_B + \frac{1}{2} M \omega_A^2 Q_A^2 \end{pmatrix}. \quad (14)$$

The electronic coupling (or resonance integral) V_{AB} term can be evaluated by a number of perturbative or supermolecular techniques.^{31–36} In this work, the coupling is calculated as half the splitting between the exciton states of the dimer.

In the original vibronic coupling model, the Hamiltonian in Eq. (14) is transformed to a symmetric basis

$$\pi_+^{(1)} = \frac{1}{\sqrt{2}} (\pi_A^{(1)} + \pi_B^{(1)}), \quad (15)$$

$$\pi_-^{(1)} = \frac{1}{\sqrt{2}} (\pi_A^{(1)} - \pi_B^{(1)}). \quad (16)$$

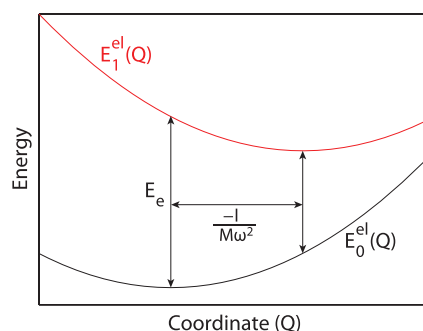


FIG. 1. Potential energy surfaces for the ground (black) and excited (red) electronic state along vibrational mode Q . E_e is the vertical excitation energy and $\frac{-l}{M\omega^2}$ is the displacement between the two minima.

This unitary transformation does not change the eigenvalues of the Hamiltonian. In addition to the electronic basis transformation, Fulton and Gouterman used a vibrational coordinate transformation from Q_A and Q_B to

$$Q_{\pm} = \frac{1}{\sqrt{2}}(Q_A \pm Q_B). \quad (17)$$

This step simplifies diagonalization of the Hamiltonian, but only when the dimer has a symmetry element ensuring $l_A = l_B$ and $\omega_A = \omega_B$.

In order to extend the model to asymmetric dimers, the transformation to the symmetric basis is not performed. By expressing momentum and position operators with raising and lowering operators and assuming a harmonic basis, the Hamiltonian matrix elements are

$$\begin{aligned} \langle \pi_A^{(1)} | H | \pi_A^{(1)} \rangle &= b_A \hbar \omega_A (\sqrt{n+1} \delta_{(n',n+1)} \\ &+ \sqrt{n} \delta_{(n',n-1)}) \delta_{(m',m)} + \left(\hbar \omega_A \left(n + \frac{1}{2} \right) \right. \\ &+ \left. \hbar \omega_B \left(m + \frac{1}{2} \right) + E_A \right) \delta_{(n',n)} \delta_{(m',m)}, \end{aligned} \quad (18)$$

$$\begin{aligned} \langle \pi_B^{(1)} | H | \pi_B^{(1)} \rangle &= b_B \hbar \omega_B (\sqrt{m+1} \delta_{(m',m+1)} \\ &+ \sqrt{m} \delta_{(m',m-1)}) \delta_{(n',n)} + \left(\hbar \omega_A \left(n + \frac{1}{2} \right) \right. \\ &+ \left. \hbar \omega_B \left(m + \frac{1}{2} \right) + E_B \right) \delta_{(n',n)} \delta_{(m',m)}, \end{aligned} \quad (19)$$

$$\langle \pi_A^{(1)} | H | \pi_B^{(1)} \rangle = \langle \pi_B^{(1)} | H | \pi_A^{(1)} \rangle = V_{AB} \delta_{(n',n)} \delta_{(m',m)}, \quad (20)$$

where n and n' (m and m') represent the excitation quanta of a given normal mode for the vibration on A (B) monomer. Dimensionless displacement parameters b_A and b_B are related to l_A and l_B as

$$b_A \hbar \omega_A = l_A \sqrt{\frac{\hbar}{2M\omega_A}}. \quad (21)$$

The expressions in Eqs. (18)–(20) are expanded in the vibrational basis. The solution generally converges rapidly, requiring around five basis functions in each vibration for spectroscopically reasonable values of b_A and b_B . Convergence with respect to the size of the basis is shown in the supplementary material.³⁷

Equations (18)–(20) can be extended in a straightforward manner for multiple vibrational modes on each monomer. In this case, each matrix element is a sum over Hamiltonians for different vibrations and the basis functions are products of the basis function from each vibration.

As pointed out by Förster and others^{16,31,38} there are different regimes of vibronic coupling: strong, weak, and intermediate. The quantity that characterizes a mode as either being strongly coupled or weakly coupled to the electronic

excitation is given as^{10,11}

$$p = \frac{2|\langle \pi_A^{(1)} | V_{AB} | \pi_B^{(1)} \rangle|}{M\omega^2 d Q^2}. \quad (22)$$

Here, $p \gg 1$ corresponds to strongly coupled systems; $p \ll 1$ characterizes weakly coupled systems. $p \simeq 1$ defines the intermediate coupling regime which exhibits the most complicated spectra. For a vibration in the strong or weak limit, it is possible to analytically compute the energies and intensities.¹⁶ Application of perturbation theory to strong and weak coupling regimes is shown in the supplementary material.³⁷ However, analytic solutions break down as the vibration enters the intermediate coupling regime. Therefore, in the present work, numerical diagonalization of the Hamiltonian using the Lanczos algorithm is employed for all cases, resulting in what Andrzejak and Petelenz call the exact numerical solution.¹⁶

B. Inter-monomer modes

To compute the eigenstates of inter-monomer vibrations, it is necessary to account for the inter-monomer kinetic energy term, T_L from Eq. (1), as well as higher order terms from the Taylor expansion of V_{AB} in Eq. (9). In order to build a total Hamiltonian, the inter-monomer Hamiltonian will be constructed in the $\{\pi_A^{(1)}, \pi_B^{(1)}\}$ basis and added onto the intra-monomer Hamiltonian. However, because the inter-monomer modes are inherently dependant on the electronic state of the dimer, it is convenient to work in the symmetrized basis $\{\pi_+^{(1)}, \pi_-^{(1)}\}$ as defined in Eqs. (15) and (16), which are the eigenvectors of the dimer electronic Hamiltonian for molecules with only a vibrational asymmetry. So, the Hamiltonian matrix elements of T_L and $V_{AB}(L)$ are first evaluated in the symmetrized basis $\{\pi_+^{(1)}, \pi_-^{(1)}\}$ and then transformed to the monomer basis $\{\pi_A^{(1)}, \pi_B^{(1)}\}$ and added to the Hamiltonian of the intra-monomer modes. In the case of a molecule that does not have electronic wavefunction symmetry, a more complicated approach to finding the relationship between the dimer electronic wavefunctions and the monomer localized electronic basis will need to be taken, but this is beyond the scope of this paper.

Since the geometries of both exciton states $\pi_+^{(1)}$ and $\pi_-^{(1)}$ are different from the ground state geometry along the inter-monomer mode L , the excited state surfaces are described as displaced parabolas. Note that the first (constant) term of the V_{AB} expansion is omitted here since it is already included in the intra-monomer mode Hamiltonian (14). Thus, for geometries near the minima of the excited states,

$$\begin{aligned} &\langle \pi_+^{(1)} | V_{AB}(L) - V_{AB}(0) + T_L | \pi_+^{(1)} \rangle \\ &= l_+ L + \frac{1}{2} M \omega_+^2 L^2 + \frac{P_+^2}{2M}, \end{aligned} \quad (23)$$

$$\begin{aligned} &\langle \pi_-^{(1)} | V_{AB}(L) - V_{AB}(0) + T_L | \pi_-^{(1)} \rangle \\ &= l_- L + \frac{1}{2} M \omega_-^2 L^2 + \frac{P_-^2}{2M}, \end{aligned} \quad (24)$$

where l_+ and l_- are the displacement parameters analogous to the l_A and l_B terms in the intra-monomer mode case. In

the dimer basis, each mode has two displacement parameters (l_+ and l_-) corresponding to the displacements in the ground state to first and second electronic excited state transitions. P_+ and P_- are the kinetic energy terms for the inter-monomer mode in the exciton states. The off-diagonal terms of the inter-monomer Hamiltonian are zero for symmetric electronic wavefunction due to the hermiticity of V_{AB} and T_L ,

$$\begin{aligned} \langle \pi_+^{(1)} | V_{AB}(L) + T_L | \pi_-^{(1)} \rangle &= \frac{1}{2} (\langle \pi_A^{(1)} | V_{AB}(L) + T_L | \pi_A^{(1)} \rangle \\ &\quad - \langle \pi_B^{(1)} | V_{AB}(L) + T_L | \pi_B^{(1)} \rangle) = 0. \end{aligned} \quad (25)$$

The reverse transformation from dimer symmetrized electronic basis into the monomer localized basis can be realized by using the following matrix equality:

$$\begin{bmatrix} \pi_A^{(1)} \\ \pi_B^{(1)} \end{bmatrix} = \frac{1}{\sqrt{2}} \begin{bmatrix} 1 & 1 \\ 1 & -1 \end{bmatrix} \begin{bmatrix} \pi_+^{(1)} \\ \pi_-^{(1)} \end{bmatrix}. \quad (26)$$

Applying this matrix transformation to the $V_{AB}(L) + T_L$ terms results in the following form of the inter-monomer mode Hamiltonian:

$$\begin{aligned} \langle \pi_A^{(1)} | V_{AB}(L) + T_L | \pi_A^{(1)} \rangle &= \langle \pi_B^{(1)} | V_{AB}(L) + T_L | \pi_B^{(1)} \rangle \\ &= \frac{1}{2} (l_+ + l_-) L + \frac{1}{2} \left(\frac{1}{2} M \omega_+^2 + \frac{1}{2} M \omega_-^2 \right) L^2, \end{aligned} \quad (27)$$

$$\begin{aligned} \langle \pi_A^{(1)} | V_{AB}(L) + T_L | \pi_B^{(1)} \rangle &= \langle \pi_B^{(1)} | V_{AB}(L) + T_L | \pi_A^{(1)} \rangle \\ &= \frac{1}{2} (l_+ - l_-) L + \frac{1}{2} \left(\frac{1}{2} M \omega_+^2 - \frac{1}{2} M \omega_-^2 \right) L^2. \end{aligned} \quad (28)$$

The Hamiltonian described in Eqs. (27) and (28) can be added to the intra-monomer mode Hamiltonian (Eqs. (18)–(20)), expanded in a vibrational basis of inter- and intra-monomer modes, and numerically diagonalized.

C. Intensities

Diagonalizing the Hamiltonian (Eqs. (18)–(20), (27) and (28)) results in the vibrational substructure of the exciton states. Evaluation of the intensities of the vibronic states in a fluorescence spectrum is discussed in this subsection. Absorption intensities can be derived analogously.

Following Fulton and Gouterman,¹⁰ the transition dipoles of a symmetric R^+ and antisymmetric R^- excited state to the

ground state are

$$\begin{aligned} R^+ &= \int \int \psi_1(q; Q, L)^* M^+ \psi_0(q; Q, L) dq \\ &\quad \phi_1(Q, L)^* \phi_0(Q, L) dQ dL, \end{aligned} \quad (29)$$

$$\begin{aligned} R^- &= \int \int \psi_1(q; Q, L)^* M^- \psi_0(q; Q, L) dq \\ &\quad \phi_1(Q, L)^* \phi_0(Q, L) dQ dL, \end{aligned} \quad (30)$$

where $\psi_1(q; Q, L)$ is the initial (excited state) electronic wavefunction of the dimer, $\phi_1(Q, L)$ is the initial vibrational wavefunction, $\psi_0(q; Q, L)$ and $\phi_0(Q, L)$ are the final (ground state) electronic and vibrational wavefunctions (the latter is not necessarily the wavefunction with no vibrational excitations). M^+ and M^- are the symmetric and antisymmetric transition dipole operators. The evaluation of R^+ shall now be demonstrated while R^- can be obtained analogously. Assuming that the electronic wavefunction is not strongly affected by the changes in vibrational coordinates, the integral over electronic coordinates and transition dipole operator may be factored out of the integral over nuclear coordinates. Expanding $\psi_1(q)$ in the vibrational basis results in

$$\begin{aligned} \psi_1(q) &= \pi_A^{(1)} \sum_n \sum_m \sum_p C_{n,m,p}^A \phi_n(Q_A) \phi_m(Q_B) \phi_p(L) \\ &\quad + \pi_B^{(1)} \sum_n \sum_m \sum_p C_{n,m,p}^B \phi_n(Q_A) \phi_m(Q_B) \phi_p(L), \end{aligned} \quad (31)$$

where $\{C_{n,m,p}^A, C_{n,m,p}^B\}$ are the expansion coefficients representing the dimer vibrational wavefunction on the basis of monomer vibrational wavefunctions. Equation (31) can be transformed into the symmetrized electronic dimer basis by applying Eq. (15). It is easy to see that the evaluation of the symmetric transition dipole moment R^+ reduces to calculation of the vibrational overlap integral and the purely electronic transition dipole moment (TDM) between the ground and symmetric excited state $\pi_+^{(1)}$,

$$\int \pi_+^{(1)} M^+ \psi_0 dq. \quad (32)$$

The transition dipole moment between the symmetric dipole operator and antisymmetric wavefunction is zero by a symmetry argument. This is explicitly shown in the supplementary material.³⁷ Thus, Eq. (29) can be rewritten as

$$\begin{aligned} R^+ &= \frac{1}{\sqrt{2}} \int \pi_+^{(1)} M^+ \psi_0(q; Q) dq \left(\int \sum_n \sum_m \sum_p C_{n,m,p}^A \phi_n(Q_A) \phi_m(Q_B) \phi_p(L) \phi_0(Q, L) dQ dL \right. \\ &\quad \left. + \int \sum_n \sum_m \sum_p C_{n,m,p}^B \phi_n(Q_A) \phi_m(Q_B) \phi_p(L) \phi_0(Q, L) dQ dL \right). \end{aligned} \quad (33)$$

The final state vibrational wavefunctions are combinations of wavefunctions corresponding to various vibrational modes, $\phi_0(Q, L) = \phi_i(Q_A)\phi_j(Q_B)\phi_k(L)$, where i, j , and k represent the excitation level on A, B, and inter-monomer vibrations, respectively. Assuming orthogonality of the vibrational wavefunctions and the parallel mode approximation,³⁹ the expression in Eq. (33) reduces to

$$R^+ = \frac{1}{\sqrt{2}} \int \pi_+^{(1)} M^+ \psi_0(q; Q) dq (C_{i,j,k}^A + C_{i,j,k}^B). \quad (34)$$

The transition dipole corresponding to the transition from the antisymmetric electronic state is

$$R^- = \frac{1}{\sqrt{2}} \int \pi_-^{(1)} M^- \psi_0(q; Q) dq (C_{i,j,k}^A - C_{i,j,k}^B). \quad (35)$$

The intensity is proportional to a square of the transition dipole moment. The total spectrum may be obtained by summing the intensities of the peaks corresponding to the symmetric and antisymmetric transitions. Note that transitions in asymmetric bichromophores may have mixed symmetric/antisymmetric character.

III. MODEL SPECTRA

In this section, general behavior of a model vibronically coupled bichromophore system is considered. In particular, spectra of asymmetric chromophores, i.e., chromophores with different vibrational frequencies or displacements of a normal mode, and spectra of inter-monomer modes are discussed. Model spectra showing the differences between the strong, weak, and intermediate coupling regimes as well as the interaction between multiple vibrations are shown in the supplementary material.³⁷ In all figures in this section and the supplementary material,³⁷ transitions through the antisymmetric TDM are shown in red while transitions through the symmetric TDM are shown in blue.

Various effects of asymmetry in intra-monomer vibrational modes are illustrated in Figs. 2–4. The asymmetry of the vibrational mode is controlled by parameter δ , with $\delta = 0$ corresponding to a symmetric vibration, i.e., vibration that is identical on monomers A and B. Figure 2 shows a case when vibrational modes on monomers have different frequencies. The interesting effect arising due to this asymmetry is splitting of the vibrational peaks in the absorption spectrum. Interestingly, the progression off the S_1 state favors the higher energy vibration while the progression off the S_2 state favors the lower energy one. The picture does not change when the symmetries of S_1 and S_2 states are switched: the lowest state exhibits the more intense progression in a high-frequency vibration. Splittings of the vibrational peaks are also observed in the corresponding emission spectra, but intensities of the split lines are almost equal.

A different case of asymmetry arises when the vibrational modes on the monomers have different displacements between the ground and excited state. Such asymmetries are expected to occur in deuterated molecules because deuteration changes the normal mode vectors, and thus the displacements to the excited state geometry. Model spectra corresponding to the mode in strong coupling regime are reported in Fig. 3. Despite the fact that the frequencies of the two vibrations are identical, the absorption spectrum shows energy splittings in the Frank-Condon progressions both off S_1 and S_2 origins. Similar to the case of the asymmetric frequencies, the lower frequency peak has lower intensity off S_1 and higher intensity off S_2 . However, unlike the case with asymmetric frequencies, the intensity of the S_1 origin and S_1 band is depleted suggesting that the vibration with higher b value is coupled to the S_1 state. Different from the case of asymmetric vibrational frequencies, no splitting is present in the emission spectra because the emission levels are governed by the ground state frequencies.

In the previous example (Fig. 3), the vibration is in the strong coupling limit. In Fig. 4, the vibrational mode with

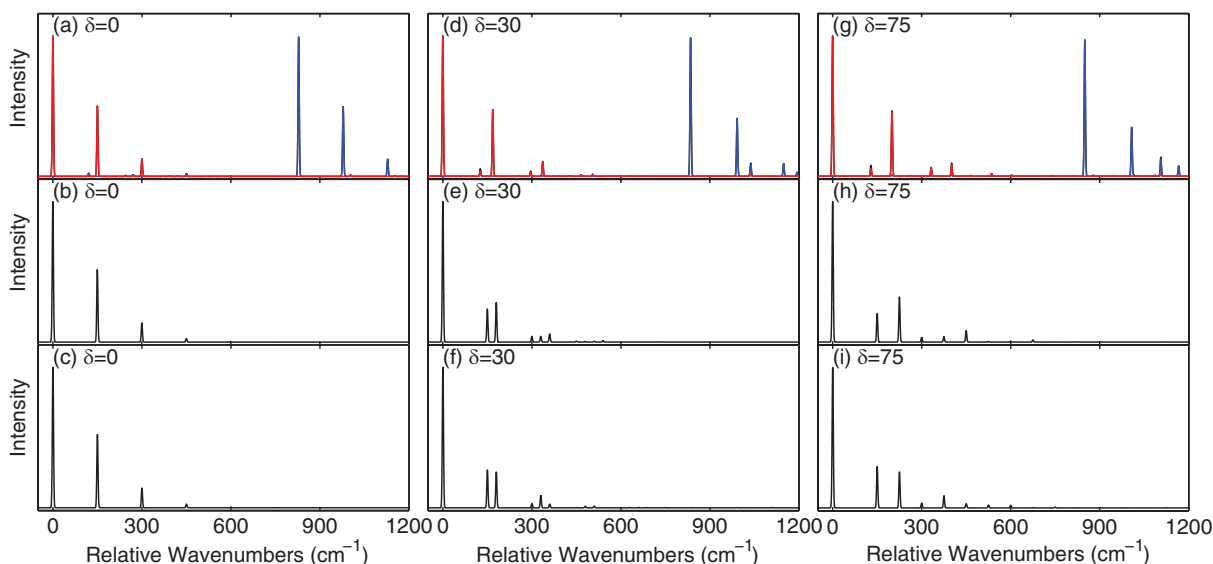


FIG. 2. Model spectra of one intra-monomer vibrational mode in strong coupling regime with different frequencies on either monomer. $\omega_A = 150 \text{ cm}^{-1}$, $\omega_B = 150 + \delta \text{ cm}^{-1}$, $b_A = b_B = 1.0$, $V_{AB} = 400 \text{ cm}^{-1}$. The first row is absorption, the second row is S_1 emission, and the third row is S_2 emission. $\delta = 0$ in (a)–(c); $\delta = 30 \text{ cm}^{-1}$ in (d)–(f); $\delta = 75 \text{ cm}^{-1}$ in (g)–(i).

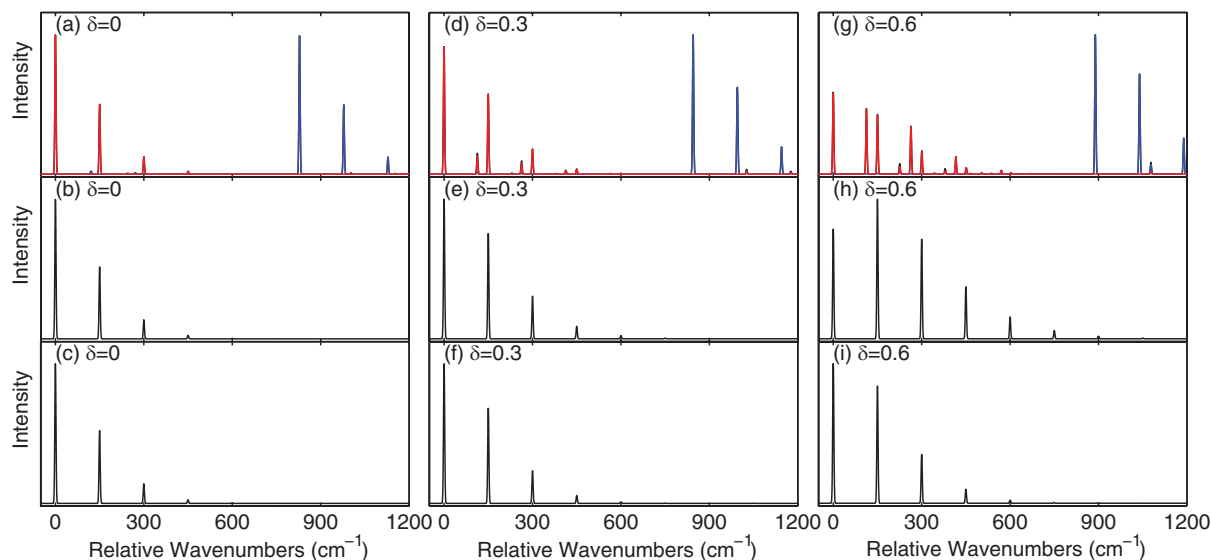


FIG. 3. Model spectra of one intra-monomer vibrational mode in strong coupling regime with different displacements on either monomer. $\omega_A = \omega_B = 150 \text{ cm}^{-1}$, $b_A = 1.0$, $b_B = 1.0 + \delta$, $V_{AB} = 400 \text{ cm}^{-1}$. The first row is absorption, the second row is S_1 emission, and the third row is S_2 emission. $\delta = 0$ in (a)–(c); $\delta = 0.3$ in (d)–(f); $\delta = 0.6$ in (g)–(i).

asymmetric displacements is placed in the weak coupling regime. In this case, the asymmetry is manifested in mixing of S_1 and S_2 progressions, i.e., as the asymmetry is increased, each peak in the absorption spectrum has a mixture of the symmetric and antisymmetric character. The peak corresponding to the S_2 origin gains intensity while the higher vibrational energy levels in the S_2 emission spectrum are reduced in intensity. Another interesting effect observed in these spectra is the increase of the splitting between the S_1 and S_2 origins upon increasing asymmetry between the modes.

Finally, the properties of the inter-monomer vibrations are examined. In the considered examples, the S_1 state is anti-symmetric and S_2 is symmetric. As discussed above, the inter-monomer vibrations may have different displacement and fre-

quency parameters for the first and second excited states of a bichromophore. In the first series of spectra, shown in Fig. 5, the effect of changing an excited state frequency is investigated. As demonstrated in Fig. 5, changing the S_1 frequency for an inter-monomer δ mode results in corresponding change in the vibrational progression off the S_1 origin, while maintaining the same vibrational pattern for the progression off the S_2 state. Both the S_1 and S_2 emission spectra retain the same vibrational spacing because these progressions are dictated by the ground state vibrational states which are independent of whether the molecule was in the S_1 or S_2 excited states.

The effect of different displacements between the $S_1 - S_0$ and $S_2 - S_0$ states (b_{S_-} and b_{S_+} parameters, respectively) is investigated in Fig. 6. When the b_{S_-} displacement is

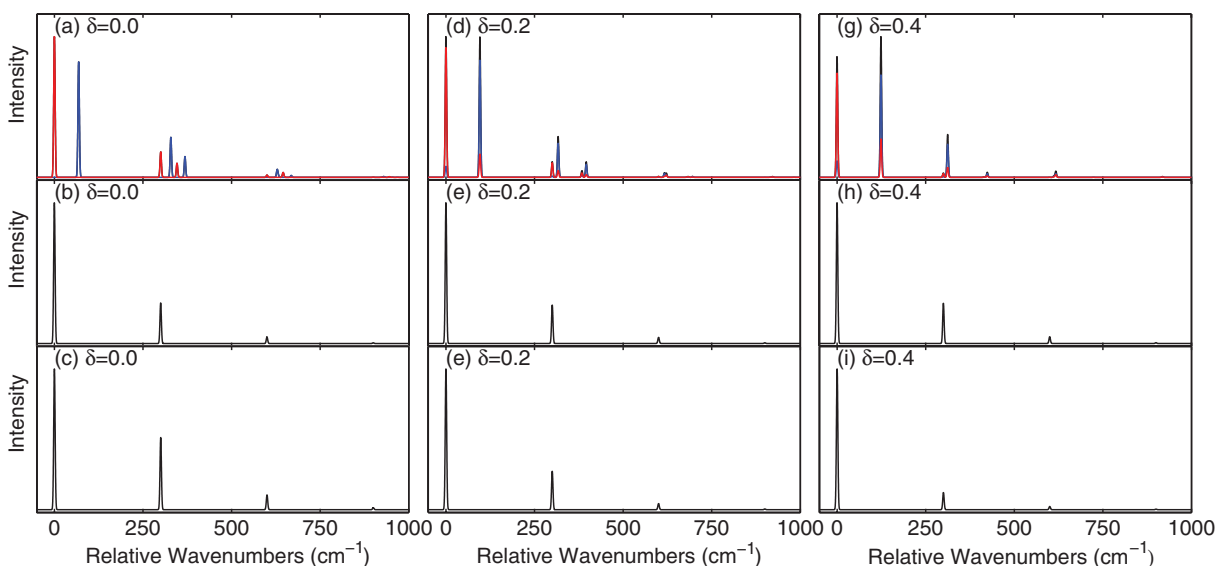


FIG. 4. Model spectra of one intra-monomer vibrational mode in weak coupling regime with different displacements on either monomer. $\omega_A = \omega_B = 300 \text{ cm}^{-1}$, $b_A = 0.6$, $b_B = 0.6 - \delta$, $V_{AB} = 50 \text{ cm}^{-1}$. The first row is absorption, the second row is S_1 emission, and the third row is S_2 emission. $\delta = 0$ in (a)–(c); $\delta = 0.2$ in (d)–(f); $\delta = 0.4$ in (g)–(i).

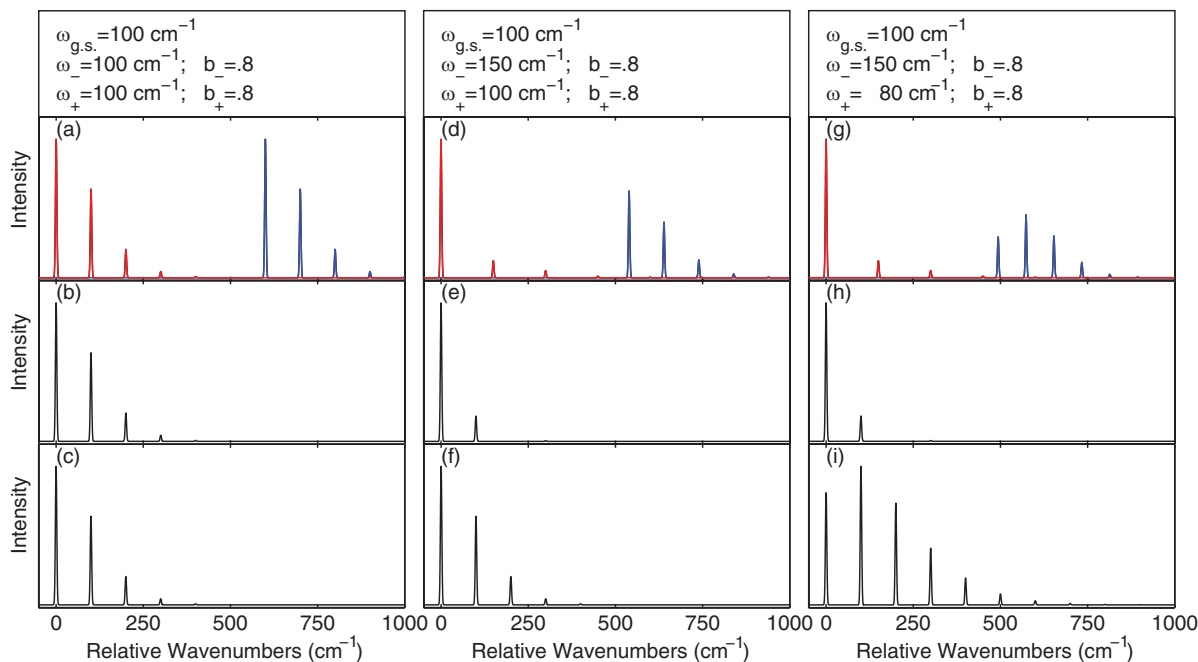


FIG. 5. Model spectra of one inter-monomer vibrational mode with different frequencies in the ground and first and second excited states of the dimer. $V_{AB} = 300 \text{ cm}^{-1}$, $b_- = b_+ = 0.8$ in all spectra. $\omega_{g,s} = \omega_- = \omega_+ = 100 \text{ cm}^{-1}$ in (a)–(c); $\omega_{g,s} = 100 \text{ cm}^{-1}$, $\omega_- = 150 \text{ cm}^{-1}$, $\omega_+ = 100 \text{ cm}^{-1}$ in (d)–(f); $\omega_{g,s} = 100 \text{ cm}^{-1}$, $\omega_- = 150 \text{ cm}^{-1}$, $\omega_+ = 80 \text{ cm}^{-1}$ in (g)–(i). The first row is absorption, the second row is S_1 (S_-) emission, and the third row is S_2 (S_+) emission. Changing the frequency of one state does not change the spacing between frequency levels for the other state.

decreased, the Frank-Condon progression off the S_1 origin in absorption and emission is depleted, while the S_2 bands remain unaffected. Similar effects are observed in the spectra of diphenylmethane, analyzed in Sec. IV. In those spectra, the low frequency inter-monomer vibrations T and \bar{T} appear in the S_1 but not S_2 fluorescence spectra.

IV. MODELING VIBRONIC SPECTRUM OF DIPHENYLMETHANE

In this section the extended FG model is applied to simulate vibronic spectra of the bichromophore DPM. Zwier and co-workers have gathered high-resolution absorption and

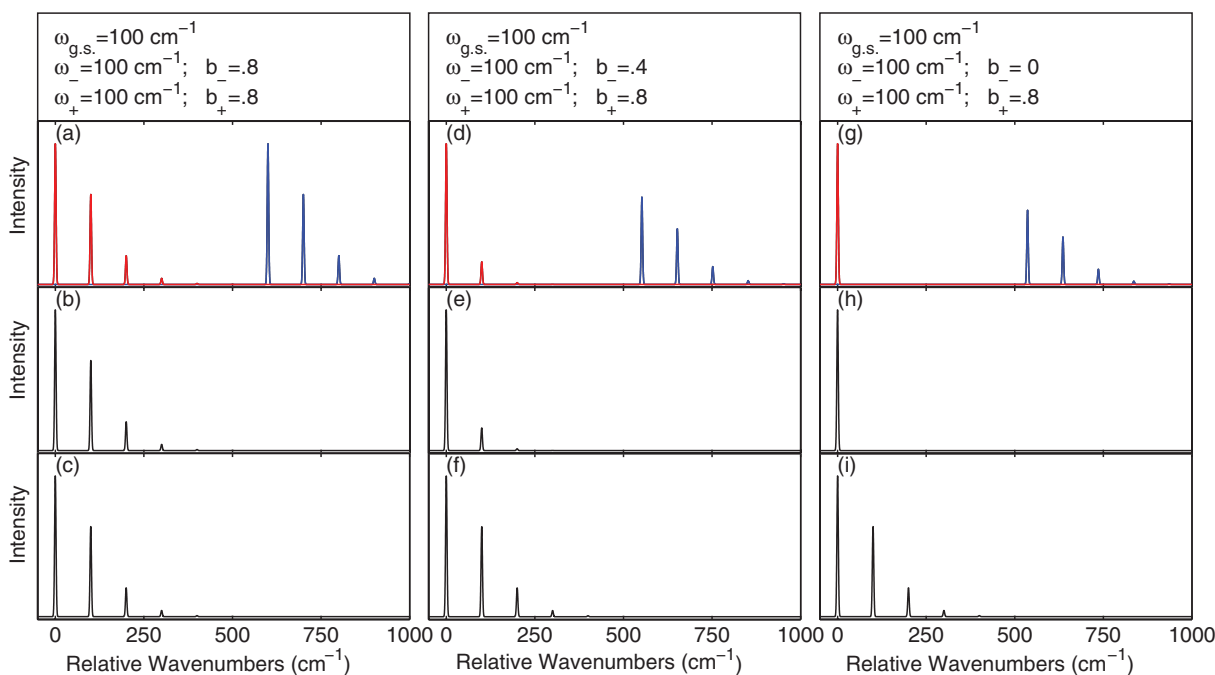


FIG. 6. Model spectra of one inter-monomer vibrational mode with different displacement parameters for the S_1 and S_2 states of the dimer. $V_{AB} = 300 \text{ cm}^{-1}$, $\omega_{g,s} = \omega_- = \omega_+ = 100 \text{ cm}^{-1}$ in all spectra. $b_- = b_+ = 0.8$ in (a)–(c); $b_- = 0.4$, $b_+ = 0.8$ in (d)–(f); $b_- = 0.0$, $b_+ = 0.8$ in (g)–(i). The first row is absorption, the second row is S_1 (S_-) emission, and the third row is S_2 (S_+) emission. Changing the displacement for one state allows to suppress the Frank-Condon progression on this state while keeping it on the other.

TABLE I. Intra-monomer vibrational parameters for diphenylmethane as found from B3LYP/cc-pVTZ calculations on toluene.

Assignment	Expt. ω^a (cm^{-1})	Calc. ω (cm^{-1})	b	p	Quenching factor ^b	Basis functions ^c
$6a_1^0$	554	530	0.26	3.4	Simulated	2
$6b_1^0$	622	639	0.43	1.1	Simulated	5
11_1^0	749	748	0.05	68	1.0	...
1_1^0	822	801	0.65	0.36	Simulated	7
12_1^0	1006	1023	0.73	0.23	0.81	...
$18a_1^0$	1035	1054	0.39	0.77	0.97	...
$9a_1^0$	1204	1206	0.43	0.54	0.89	...
$19b_1^0$	1447	1535	0.02	129	1.0	...

^aDPM experimental frequencies from Ref. 29.

^bQuenching factors used to compute the effective electronic coupling as in Eq. (36) for modes not directly included in the simulation ("simulated"). The product of all quenching factors is $\prod_{i=1}^N e^{-b_i^2} = 0.48$.

^cNumber of vibrational basis functions used in modeling.

emission spectra of the first two singlet excited states of DPM and we will follow their notations for labeling the DPM vibrational modes.²⁹

A. Computational details

Vibrational frequencies and displacement parameters for each vibration as well as an electronic coupling term and relative transition dipole moments of S_1 and S_2 are required as input for the vibronic model. The parameters for intra-monomer modes were obtained from density functional theory (DFT) and time-dependent density functional theory (TD-DFT) calculations on toluene which is considered to be a "monomer" of diphenylmethane. The ground and first excited state geometries of toluene were optimized with B3LYP functional⁴⁰⁻⁴² in the cc-pVTZ basis set⁴³ with the Q-Chem electronic structure package.⁴⁴ Vibrational frequencies of the ground state of toluene were obtained at the same level of theory. ezSpectrum software⁴⁵ was used to find the displacements between the ground and first excited state geometries on the basis of the ground state vibrational vectors. These displacements were converted into b parameters; the normal modes with the largest b parameters and corresponding p values (Eq. (22)) are listed in Table I. The number of vibrational basis functions needed for convergence for different b values is determined from extensive testing shown in supplementary material.³⁷

To obtain the parameters for the inter-monomer modes, one needs to perform electronic structure calculations on the S_0 , S_1 , and S_2 states of the dimer (DPM). The parameters obtained from DFT and TD-DFT B3LYP/cc-pVTZ computations are summarized in Table II. The experimental spectra of DPM reveal progressions along five low-frequency inter-monomer modes: symmetric and antisymmetric torsions T and \bar{T} , symmetric and antisymmetric R and \bar{R} modes, and the butterfly mode β (shown in supplementary material³⁷). From those, parameters of R and \bar{R} were computed in a standard way, i.e., S_0 , S_1 , and S_2 states of DPM were optimized (the constrained optimization with fixed values of torsional angle corresponding to the T mode was employed for S_2), then the

TABLE II. Inter-monomer vibrational parameters as found from B3LYP/cc-pVTZ calculations on S_0 , S_1 , and S_2 states of diphenylmethane.

Assignment	$\omega_{S_0}(\omega_{g.s.})$ (cm^{-1})	$\omega_{S_1}(\omega_-)$ (cm^{-1})	$\omega_{S_2}(\omega_+)$ (cm^{-1})	$b_{S_1}(b_-)$	$b_{S_2}(b_+)$
\bar{T}	22.5	38.3	... ^a	-0.02	-0.06
T	38.5	47.9	35.2	0.60	0.60
β	68.1	62.0	67.5	-1.0	1.2
\bar{R}	191	192	105	0.0	0.0
R	225	202	157	-0.62	-0.08

^aNo real-value frequency could be obtained.

displacements between the ground and the first and second excited state geometries were found on the basis of the ground state vibrations.

Due to an anharmonic nature of the other three modes and extreme sensitivity of parameters to the level of theory employed, their parameters were obtained from PES calculations. Namely, potential energy slices were constructed along normal mode vectors of each mode starting from the S_1 state geometry and employing $0.002 \text{ \AA} \sqrt{\text{amu}}$ displacement increments in either direction of the vibrational vector. TD-DFT B3LYP/cc-pVTZ calculations were performed to find energies of S_1 and S_2 states at each of these geometries. For each vibration, the S_1 and S_2 energies were fit to parabolas, from which frequency and displacement parameters were extracted. As an example, plots of the energies and parabolic fits for the T mode are shown in Fig. 7. However, while this procedure improved agreement between experimental and calculated values of the low-frequency modes compared to the direct calculation of Hessians of the S_1 and S_2 states, it still resulted in overestimated frequencies for all modes and strongly overestimated displacement for the β mode. It should be noted, however, that the β mode is governed by an interplay of covalent and non-covalent, in particular dispersion, interactions between the aromatic rings, and as such is extremely sensitive to the level of theory.

In order to improve the agreement with the experimental spectra, some of the parameters for inter-monomer modes were adjusted. The butterfly mode β that reveals very little intensity in the experimental spectra was excluded from modeling. The resulting set of inter-monomer parameters is presented in Table III.

Vertical splittings between the first and second electronic excited states of DPM were computed by a number of electronic structure methods, including TD-DFT with various functionals (B3LYP, BP86,^{46,47} and long-range and

TABLE III. Adjusted (fitted to experimental spectra) inter-monomer vibrational parameters. Calculated values were kept where appropriate.

Assignment	$\omega_{S_0}(\omega_{g.s.})$ (cm^{-1})	$\omega_{S_1}(\omega_-)$ (cm^{-1})	$\omega_{S_2}(\omega_+)$ (cm^{-1})	$b_{S_1}(b_-)$	$b_{S_2}(b_+)$	Basis functions ^a
\bar{T}	10.0	23.0	10.0	-0.02	-0.06	8
T	20.0	28.3	20.0	1.40	0.0	12
\bar{R}	191	275	105	0.0	0.0	3
R	225	285	188	-0.55	-0.08	7

^aNumber of vibrational basis functions used in modeling.

TABLE IV. Vertical $S_1 - S_2$ splittings computed at the ground state optimized geometry.^a

Level of theory	$S_1 - S_2$ splitting (cm^{-1})
EOM-CCSD/cc-pVDZ	430
ω B97X-D/cc-pVTZ	549
BP86/cc-pVTZ	539
B3LYP/cc-pVTZ	1069

^aMP2/cc-pVTZ ground state geometry was used in these calculations.

dispersion corrected ω B97X-D (Ref. 48)), and equation-of-motion coupled cluster with single and double excitations method^{49–52} (EOM-CCSD) (see Table IV). Apparently, the value of splitting is sensitive to the level of theory, with the best estimates provided by EOM-CCSD and TD-DFT with ω B97X-D. This results in the electronic coupling, taken as a half of the splitting, in the range of 215 – 275 cm^{-1} . Including quenching factor due to high-frequency (weakly-coupled) vibrational modes not explicitly included in the simulation (see Table I) results in the effective electronic coupling

$$V_{AB}^{eff} = V_{AB} \prod_{i=1}^N e^{-\frac{b_{A,i}^2}{2}} e^{-\frac{b_{B,i}^2}{2}} = V_{AB} \prod_{i=1}^N e^{-b_i^2}, \quad (36)$$

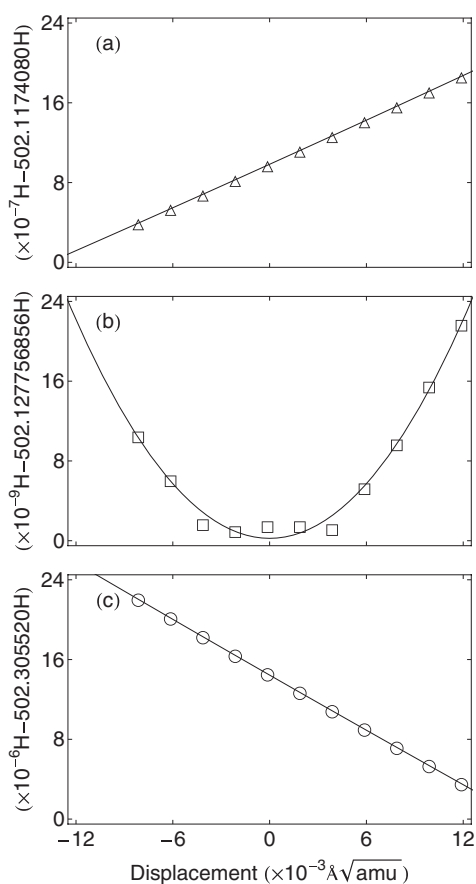


FIG. 7. Potential energy surfaces of the symmetric torsion T mode in (a) the second excited state, (b) the first excited state, and (c) the ground state. The abscissa is the displacement from the optimized S_1 geometry. Energy scales in frames (a)–(c) are different because near the S_1 minimum, the PES of the S_1 state is dominated by second order effects while PESs of the other two states are dominated by first order effects.

where $b_{A,i}$ and $b_{B,i}$ are displacements for the i th mode on monomer A and B, respectively. In the symmetric case, as in DPM, $b_{A,i} = b_{B,i}$. Using the parameters in Table I, this results in an effective coupling in the range of 103 – 132 cm^{-1} . The coupling constant used for modeling DPM spectra was taken as 155.8 cm^{-1} . All simulated peaks were modeled by Gaussians with a standard deviation of 1 cm^{-1} .

B. DPM spectra

Using simulated parameters for intra-monomer vibrational modes (Table I), partly fitted parameters for inter-monomer vibrational modes (Table III), and effective coupling constant $V_{AB} = 155.8 \text{ cm}^{-1}$, theoretical spectra for DPM were computed as shown in Fig. 8. Comparison of the experimental and theoretical low-frequency absorption spectra (Fig. 8(a)) shows a quantitative agreement both in peak positions and intensities. In particular, one can clearly recognize a progression along the torsional mode T , with peaks at 27, 54, and 81 cm^{-1} . The peak at 43 cm^{-1} is the second vibrational state of \bar{T} (i.e., \bar{T}^2), while the first vibrational quanta are not present. This is because the intensity in the \bar{T} mode is originated due to a frequency change rather than a displacement between the electronic states. Therefore, only even quanta of this mode gain non-zero intensity. Small displacement along the \bar{T} mode ensures that the electronic transition dipole moment that is formally dependent on this mode stays constant and the Condon approximation (Eqs. (34) and (35)) is valid.

As follows from decomposition of the absorption spectrum into symmetric and antisymmetric components (Fig. 8(b)), the origin of the second excited state appears at about 123 cm^{-1} , in agreement with experimental assignment. The intensity of S_2 origin is well reproduced by a S_1/S_2 TDM ratio of 2.08 : 1, which is in close agreement with the 1.98 : 1 ratio computed at the ω B97X-D/cc-pVTZ level of theory.

Analysis of the emission spectrum from the S_1 origin (Fig. 8(c)) shows that the peak at 63 cm^{-1} , missing in the simulated spectrum, is due to the β mode that was excluded from simulations, as mentioned above. Another inter-monomer vibration, R , reveals itself in an intense line at 221 cm^{-1} . This peak is well reproduced by the *ab initio* computations, with only a minor correction in the displacement parameter. All intra-monomer modes, $6a_1^0$, $6b_1^0$, and 1_1^0 , are reasonably well described by *ab initio* calculations, with frequency discrepancies not exceeding 30 cm^{-1} . The 11_1^0 vibration with frequency 748 cm^{-1} was not included in the calculation due to a lack of intensity in the S_2 emission spectrum (Fig. 8(d)). There is also a nice agreement between theory and experiment in the high-frequency peaks due to intra-monomer vibrations in the emission spectrum of the S_2 origin (Fig. 8(d)). It is very encouraging that the model spectrum accurately predicts the change in intensity of vibronic bands in the S_1 and S_2 emission spectra, even though there is no parameter that directly controls that intensity ratio.

The obviously missing part of the modeled S_2 emission spectrum is the so called “clump” emission around 100 cm^{-1} . As proposed by Zwier and co-workers, these bands are not

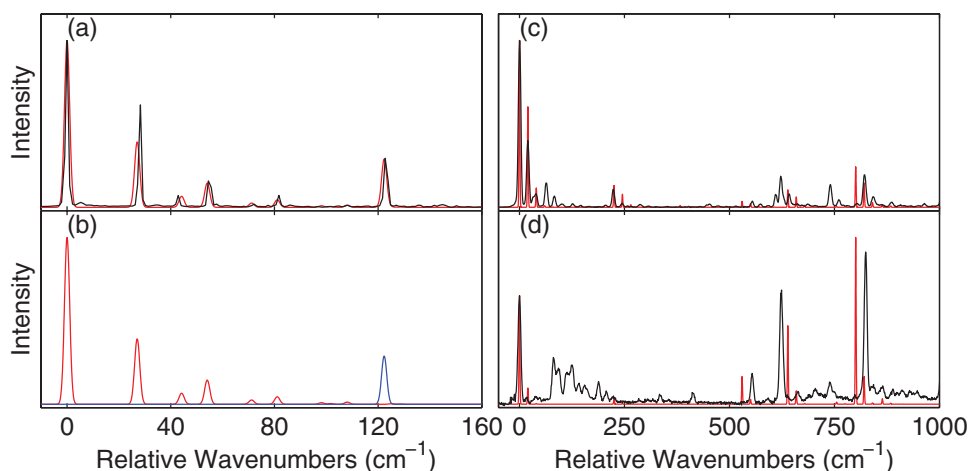


FIG. 8. DPM spectra produced from parameters in Tables I and III with an electronic coupling constant of 155.8 cm^{-1} . Comparison of the calculated (red) and experimental (black) absorption spectra is shown in (a). Breakdown of the calculated spectrum by the electronic state, with the red trace representing the S_1 (anti-symmetric) state and the blue trace representing the S_2 (symmetric) state in (b). (c) and (d) Comparisons of the calculated (red) and experimental (black) emission spectra from the S_1 and S_2 origins, respectively.

vibronic progressions off the S_2 state but emissions from the S_1 vibrational bands that gain their intensity due to the energetic proximity to the S_2 origin.²⁹ Indeed, the simulation produces two vibronic S_1 states (with very low intensity) within $\pm 10 \text{ cm}^{-1}$ of the S_2 origin. One of them is mainly composed of $T^3\bar{T}^3$ hot band, and another one is a mixture of $T^5\bar{T}$ and $T^6\bar{T}$. We mimicked the “clump” emission spectrum by producing emission spectra from these two vibronic states and adding them in equal proportions, and fitting the intensity of the combined spectra to the experimental “clump” emission. The resulting spectrum is provided in Fig. 9. The modeled “clump” spectrum qualitatively reproduces the experimental emission in the region $0\text{--}200 \text{ cm}^{-1}$, with a low-intensity region from $0\text{--}80 \text{ cm}^{-1}$ followed by a clump of peaks. Thus, our results are in accord with assignments suggested by Zwier.²⁹

V. CONCLUSIONS

The vibronic model has been extended to treat asymmetric molecules and inter-chromophore vibrational modes. Several vibrational modes can be considered simultaneously by

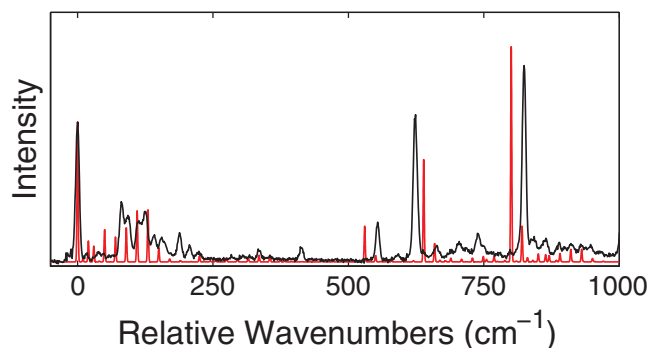


FIG. 9. S_2 “clump” emission spectra. The calculated spectrum (in red) is produced by adding S_2 emission spectrum as in Fig. 8(d) with emissions from energetically close S_1 vibrational states. Experimental spectrum is in black.

means of Lanczos diagonalization of the sparse Hamiltonian matrix. Considered model spectra provide detailed analysis of the theory, including effects of simultaneous modeling of several modes and effects of asymmetries in different kinds in intra- and inter-monomer vibrations.

Modeling of the vibronic spectra of DPM demonstrates applicability of the developed model to real-life bichromophores. It is found that obtaining accurate parameters for the FG model may be challenging, especially parameters for the low-frequency inter-monomer modes that require computations of optimal geometries and vibrational frequencies of a bichromophore. However, inclusion of the inter-monomer modes is essential for modeling spectra of flexible bichromophores. Using the computed parameters for the intra-monomer modes and partly fit parameters for the inter-monomer modes, the experimental absorption and emission spectra of DPM were successfully reproduced. Additionally, a qualitative modeling of the clump emission spectrum was provided, even though a more rigorous theoretical framework may be needed in order to provide physically meaningful rather than fit representation of this region.

Future work will include applications of the developed model to asymmetrically deuterated diphenylmethane and other related asymmetrically substituted bichromophores, as well as extensions of the vibronic model to electronic asymmetries and tri- and multi-chromophore complexes.

ACKNOWLEDGMENTS

This work was supported by National Science Foundation (NSF) Career Grant No. CHE-0955419 and Purdue Research Foundation. B.N. was partly supported by Andrews Graduate Fellowship. The authors thank Professor Tim Zwier, Dr. Christian Müller, and Dr. David Plusquellic for many fruitful discussions related to this work.

¹M. Born and R. Oppenheimer, *Ann. Phys.* **84**, 0457 (1927).

²G. A. Worth and L. S. Cederbaum, *Annu. Rev. Phys. Chem.* **55**, 127 (2004).

³J. C. Tully, *Int. J. Quantum Chem.* **40**, 299 (1991).

- ⁴P. Ehrenfest, *Z. Phys. A: Hadron Nucl.* **45**, 455 (1927).
- ⁵H.-D. Meyer and W. H. Miller, *J. Chem. Phys.* **70**, 3214 (1979).
- ⁶U. Manthe, H.-D. Meyer, and L. S. Cederbaum, *J. Chem. Phys.* **97**, 3199 (1992).
- ⁷R. Kosloff, *J. Phys. Chem.* **92**, 2087 (1988).
- ⁸A. Witkowski and W. Moffitt, *J. Chem. Phys.* **33**, 872 (1960).
- ⁹R. L. Fulton, *J. Chem. Phys.* **56**, 1210 (1970).
- ¹⁰R. L. Fulton and M. Gouterman, *J. Chem. Phys.* **35**, 1059 (1961).
- ¹¹A. Witkowski, in *Modern Quantum Chemistry*, edited by O. Sinanoğlu (Academic, New York, 1965), Vol. III.
- ¹²A. R. Gregory, W. H. Henneker, W. Siebrand, and M. Z. Zgierski, *J. Chem. Phys.* **63**, 5475 (1975).
- ¹³W. Siebrand, *J. Chem. Phys.* **40**, 2223 (1964).
- ¹⁴P. Petelenz and M. Andrzejak, *J. Chem. Phys.* **113**, 11306 (2000).
- ¹⁵K. Sakota and H. Sekiya, *J. Phys. Chem. A* **109**, 2718 (2005).
- ¹⁶M. Andrzejak and P. Petelenz, *Chem. Phys.* **335**, 155 (2007).
- ¹⁷P. Ottiger, S. Leutwyler, and H. Koppel, *J. Chem. Phys.* **131**, 204308 (2009).
- ¹⁸C. G. Heid, P. Ottiger, R. Leist, and S. Leutwyler, *J. Chem. Phys.* **135**, 154311 (2011).
- ¹⁹C. P. Rodrigo, C. W. Müller, N. R. Pillsbury, W. H. James III, D. F. Plusquellic, and T. S. Zwier, *J. Chem. Phys.* **134**, 164312 (2011).
- ²⁰A. M. Kelley, *J. Chem. Phys.* **119**, 3320 (2003).
- ²¹J. Guthmuller, F. Zutterman, and B. Champagne, *J. Chem. Theory Comput.* **4**, 2094 (2008).
- ²²J. Guthmuller, F. Zutterman, and B. Champagne, *J. Chem. Phys.* **131**, 154302 (2009).
- ²³J. Seibt, V. Dehm, F. Wuerthner, and V. Engel, *J. Chem. Phys.* **126**, 164308 (2007).
- ²⁴F. C. Spano and L. Silvestri, *J. Chem. Phys.* **132**, 094704 (2010).
- ²⁵C. Woywod, W. Domcke, A. L. Sobolewski, and H.-J. Werner, *J. Chem. Phys.* **100**(2), 1400 (1994).
- ²⁶M. Feigel, *J. Mol. Struct.: THEOCHEM* **366**, 83 (1996).
- ²⁷R. Coffman and D. S. McClure, *Can. J. Chem.* **36**, 48 (1958).
- ²⁸D. S. McClure, *Can. J. Chem.* **36**, 59 (1958).
- ²⁹N. R. Pillsbury, J. A. Stearns, C. W. Müller, D. F. Plusquellic, and T. S. Zwier, *J. Chem. Phys.* **129**, 114301 (2008).
- ³⁰J. A. Stearns, N. R. Pillsbury, K. O. Douglass, C. W. Müller, T. S. Zwier, and D. F. Plusquellic, *J. Chem. Phys.* **129**, 224305 (2008).
- ³¹T. Förster, in *Modern Quantum Chemistry*, edited by O. Sinanoğlu (Academic, New York, 1965), Vol. III.
- ³²C.-P. Hsu, G. R. Fleming, M. Head-Gordon, and T. Head-Gordon, *J. Chem. Phys.* **114**, 3065 (2001).
- ³³C.-P. Hsu, *Acc. Chem. Res.* **42**, 509 (2009).
- ³⁴J. E. Subotnik, J. Vura-Weis, A. J. Sodt, and M. A. Ratner, *J. Phys. Chem. A* **114**, 8665 (2010).
- ³⁵G. D. Scholes and K. P. Ghiggino, *J. Phys. Chem.* **98**, 4580 (1994).
- ³⁶J.-L. Bredas, D. Beljonne, V. Coropceanu, and J. Cornil, *Chem. Rev.* **104**, 4971 (2004).
- ³⁷See supplementary material at <http://dx.doi.org/10.1063/1.4747336> for analysis of the convergence of vibronic spectra with a size of the vibrational basis, application of the perturbation theory to the strong and weak coupling limits, and visualization of the DPM inter-monomer vibrations.
- ³⁸E. G. McRae and W. Siebrand, *J. Chem. Phys.* **41**, 905 (1964).
- ³⁹E. Condon, *Phys. Rev.* **28**, 1182 (1926).
- ⁴⁰C. Lee, W. Yang, and R. G. Parr, *Phys. Rev. B* **37**, 785 (1988).
- ⁴¹S. H. Vosko, L. Wilk, and M. Nusair, *Can. J. Phys.* **58**, 1200 (1980).
- ⁴²A. D. Becke, *J. Chem. Phys.* **98**, 1372 (1993).
- ⁴³J. Thom and H. Dunning, *J. Chem. Phys.* **90**, 1007 (1989).
- ⁴⁴Y. Shao, L. Molnar, Y. Jung, J. Kussmann, C. Ochsenfeld, S. Brown, A. Gilbert, L. Slipchenko, S. Levchenko, D. O'Neil, R. DiStasio, Jr., R. Lochan, T. Wang, G. Beran, N. Besley, J. Herbert, C. Lin, T. Van Voorhis, S. Chien, A. Sodt, R. Steele, V. Rassolov, P. Maslen, P. Korambath, R. Adamson, B. Austin, J. Baker, E. Bird, H. Daschel, R. Doerksen, A. Drew, B. Dunietz, A. Dutoi, T. Furlani, S. Gwaltney, A. Heyden, S. Hirata, C.-P. Hsu, G. Kedziora, R. Khalliulin, P. Klunziger, A. Lee, W. Liang, I. Lotan, N. Nair, B. Peters, E. Proynov, P. Pieniazek, Y. Rhee, J. Ritchie, E. Rosta, C. Sherrill, A. Simmonett, J. Subotnik, H. Woodcock III, W. Zhang, A. Bell, A. Chakraborty, D. Chipman, F. Keil, A. Warshel, W. Herbe, H. Schaefer III, J. Kong, A. Krylov, P. Gill, and M. Head-Gordon, *Phys. Chem. Chem. Phys.* **8**, 3172 (2006).
- ⁴⁵V. Mozhaykiy and A. Krylov, ezSpectrum, see <http://iopshell.usc.edu/downloads/>.
- ⁴⁶J. P. Perdew, *Phys. Rev. B* **33**, 8822 (1986).
- ⁴⁷A. D. Becke, *Phys. Rev. A* **38**, 3098 (1988).
- ⁴⁸J.-D. Chai and M. Head-Gordon, *Phys. Chem. Chem. Phys.* **10**, 6615 (2008).
- ⁴⁹J. F. Stanton and R. J. Bartlett, *J. Chem. Phys.* **98**, 7029 (1993).
- ⁵⁰H. Sekino and R. J. Bartlett, *Int. J. Quantum Chem.* **26**, 255 (1984).
- ⁵¹H. Koch, H. J. A. Jensen, P. Jørgensen, and T. Helgaker, *J. Chem. Phys.* **93**, 3345 (1990).
- ⁵²A. Krylov, *Annu. Rev. Phys. Chem.* **59**, 433 (2008).